

Online Feedback Optimization for Subtransmission Grid Control

Lukas Ortmann, Jean Maeght, Patrick Panciatici, Florian Dörfler, Saverio Bolognani

Abstract—The increasing electric power consumption and the shift towards renewable energy resources demand for new ways to operate transmission and subtransmission grids. Online Feedback Optimization (OFO) is a feedback control method that enables real-time, constrained, and optimal control of these grids. Such controllers can minimize, e.g., curtailment and losses while satisfying grid constraints like voltage and current limits. We tailor and extend the OFO control method to handle discrete inputs and explain how to design an OFO controller for the subtransmission grid. We present a novel and publicly available benchmark which is of the real French subtransmission grid on which we analyze the proposed controller in terms of robustness against model mismatch, constraint satisfaction, and tracking performance. Overall, we show that OFO controllers can help utilize the grid to its full extent, virtually reinforce it, and operate it optimally and in real-time by using flexibility offered by renewable generators connected to distribution grids.

I. INTRODUCTION

More and more renewable power is installed in the grid to achieve the climate goals [1], [2] and energy independence. In some areas, the capacity of the grid is partly reached and renewable power needs to be curtailed to mitigate overloaded lines [3] and overvoltages. The typical approach to prevent overloaded lines is to curtail the renewable generation to a fixed maximum value, depending on the seasonal thermal ratings of the lines, without taking consumption and other generation into account. For example, these actions currently need to be implemented in the Blocaux area in France which we will use as a benchmark in this paper. However, this solution leads to unnecessary curtailment of renewable generation [3]. The current practice for voltage control depends on the country and ranges from manual to automatic control with large sampling times. The fast-changing power injections of renewable energy sources like wind and solar require higher control rates to enforce voltage and current limits in the grid. Because of this, manual operation strategies or automatic control with sampling times in the minutes will be incapable of safely operating a highly loaded, uncertain, and variable grid in the future. This problem is becoming more severe with increasing renewable integration and is affecting more areas of power grids worldwide [3]. Hence, increasing real-time automation is needed with control actions taken every few seconds.

Lukas Ortmann, Florian Dörfler, and Saverio Bolognani are with the Automatic Control Laboratory at ETH Zurich, Zurich, Switzerland. Emails: {ortmannl,dorfler,bsaverio}@ethz.ch

Jean Maeght and Patrick Panciatici are with Réseau de Transport d'Électricité (RTE), Paris, France. Email: firstname.lastname@rte-france.com

Funding by the Swiss Federal Office of Energy through the project "UNICORN" (SI/501708) is gratefully acknowledged.

Real-time control does not only allow to operate the grid under variable renewable generation, but it can also mitigate the need to physically reinforce the grid by virtual reinforcement through automatic control. A report by the French transmission grid operator RTE estimates possible savings of 7 billion Euros over 10 years through using real-time control for active power instead of building new power lines [3]. This opportunity comes from the higher degree of controllability of the grid, given by the flexibility of a fine network of renewable generators connected to almost every bus. Virtual grid reinforcement can be phrased as an optimization problem. However, such optimization is inherently an offline decision-making method, e.g., solving an Optimal Power Flow (OPF) problem and deploying the solution on the grid, see Figure 1. This is a feedforward control approach that lacks robustness to unknown disturbances and model uncertainties. Further, it is difficult to run in real-time and can be (at best) implemented repeatedly. While some degree of uncertainty can be tackled via robust optimization tools, such an approach would increase the computational load (thus leading to longer sampling rates) and would jeopardize the efficiency of the solution (due to prioritizing robustness against model mismatch). In contrast, Online Optimization approaches have been analyzed for power system problems, see [4]. Online Optimization methods combine feedback-based real-time control and optimal operation with respect to an optimization problem. An Online Optimization controller tracks the solution of a nonlinear optimization problem that, at each time, depends on the instantaneous availability of generation, loads, etc. From a control perspective, we want to design a control policy so that this optimal state is an attractive equilibrium for the controlled power grid. We choose the Online Optimization method, called OFO to steer the grid to the optimal operating point using feedback, see Figure 1. This method was specifically developed to drive power systems to the solution of an optimization problem while guaranteeing constraint satisfaction [5]–[10]. It needs minimal model information, and it was experimentally validated in different distribution microgrids [11]–[13].

Related earlier works also use Online Optimization and optimization algorithms as feedback controllers to drive a power system to an optimal operation point. Such algorithms have been analyzed for optimal frequency control, optimal voltage control, and optimal power flow, see [4] for an extensive review. Most papers analyze the Volt/VAR problem, e.g. [14]–[16] and until now nearly all publications have dealt with distribution grids, e.g. [17]–[21]. Recently, the publication [22] analyzed such algorithms for transmission grids but again only consider voltage control. For a distribution grid setup the

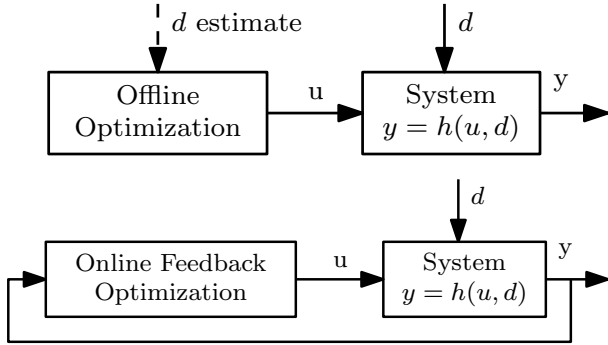


Fig. 1: Offline vs. Online Feedback Optimization.

authors of [23] include tap changers in their algorithm but again only voltage control is considered.

Overall, the Online Optimization algorithms are mostly used for voltage control in distribution grids and up until now are, except one, limited to continuous inputs whereas inputs in a real power grid can also be discrete, e.g. tap changers. Furthermore, most of them assume to have perfect model information and only consider a subset of available control inputs. Also, synthetic grid models are usually used to analyze the performance. However, these models lack important properties of real power grids e.g., locally controlled tap changers or independently operating voltage-controlled generators. Therefore, important features of these algorithms like constraint satisfaction, tracking of a time-varying optimum, and robustness to model mismatch have not yet been analyzed on a real grid benchmark which is essential to pave the way toward a deployment. In summary, previous approaches to OFO for voltage control had an academic focus, considered synthetic case studies, and relied upon idealistic assumptions. Our contributions are to present and make publicly available a novel subtransmission benchmark model that represents the real French transmission and subtransmission grid. We extend and tailor OFO methods with the capability to handle discrete actuators like tap changers and demonstrate how such controllers can be tuned. We design a uniform controller utilizing active and reactive power injections as well as tap changers. On the provided benchmark, we show the tracking performance, the constraint satisfaction, and the robustness to model mismatch of our OFO controller, and compare it to Offline Optimization.

II. THE UNICORN 7019 BENCHMARK

In this section, we present the Unicorn 7019 benchmark which is a real benchmark in the French subtransmission grid. We use it to show the performance of our OFO controller. The benchmark is implemented in MATPOWER [24] and Matlab Simulink through the toolbox SimulinkMATPOWER [25]. The grid model for the benchmark is the real French transmission and subtransmission grid, which consists of 7019 buses, 9657 branches, 1465 generators, and 907 tap changers. We simulate the steady-state behavior of the whole grid. That means whenever the controller has updated its control setpoints u , a power flow is solved. Afterward, all tap changers, which

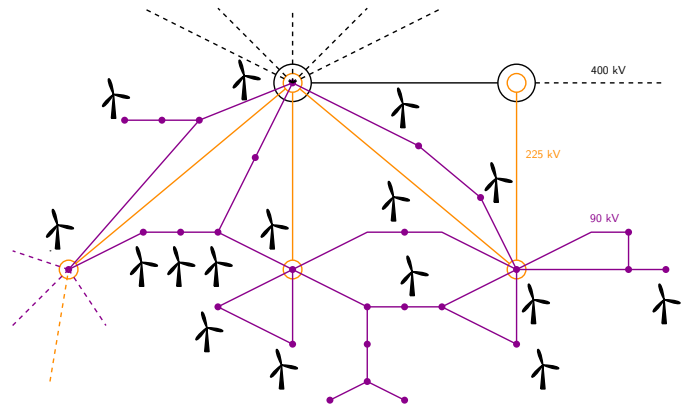


Fig. 2: The Blocaux area with 31 buses, 58 branches, and 42 wind farms with a total power of 1274 MW. Connections to the rest of France are indicated with dashed lines. The tap changers are on the transformers connecting the different voltage levels.

are not controlled by our controller, determine whether their secondary voltage is within bounds. Otherwise, they switch taps and the power flow is solved again with the updated tap ratios. This is done iteratively until no further tap changes occur. This mimics the operating behavior of the real power system. Figure 2 shows the Blocaux area, which is located in the north of France. The wind power exceeds the capacity of the grid, and during the summer of 2021, the wind farms were curtailed at a fixed level to prevent overloaded lines. This sometimes leads to unnecessary curtailment.

The task in the benchmark is to minimize the losses and active power curtailment in the Blocaux area using the active and reactive power injections of the wind farms and the on-load tap changers, while satisfying the grid constraints, i.e., voltage magnitude limits at the buses and power flow limits on the lines. During the simulation the wind power produced by the wind farms is changing rapidly, see the blue line in the upper right panel of Figure 4. This leads to a time-varying optimum that the controller has to track while guaranteeing the satisfaction of the constraints. For the wind profile, we use real measurements from a wind farm taken in a location close to the Blocaux area. We chose this specific wind profile because the fast change of power makes tracking the optimum difficult and satisfying the constraints hard.

The Blocaux area consists of 31 buses, 58 branches, and there are 10 on-load tap changers on the transformers between the transmission grid (225 kV and 400 kV) and the subtransmission grid (90 kV). There are 42 wind farms with power ratings between 0.5 MW and 102 MW, and a total installed wind power of 1274 MW. We assume the active and reactive power of the 42 wind farms and the position of all 10 tap changers can be controlled. The control architecture can be seen in Figure 3 and is as follows. Measurement devices take voltage magnitude measurements v and measure the absolute value of the complex power flow ℓ , respectively. These are sent to a centralized location, a regional SCADA system, or one of the substations, where the controller is implemented. The controller calculates the reactive and active power setpoints

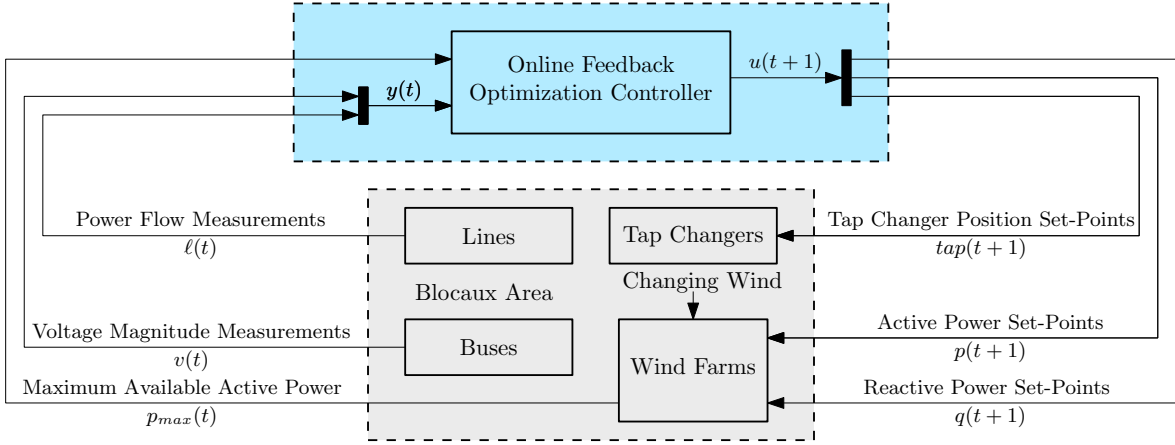


Fig. 3: Block diagram of the control setup with the controller in blue and the grid in gray.

and tap changer positions. These are then communicated to the wind farms and tap changers. Note, that the wind farms accept continuous setpoints, whereas the tap changers are discrete actuators and only accept 33 equally spaced values between 0.9 and 1.1. We assume that the wind farms cannot only accept setpoints, but they can also communicate the currently available wind power to the controller. This could for example be based on a wind speed measurement. To showcase the capabilities of the controller, we define two tasks with which we challenge the controller.

Optimal and Safe Curtailment: The goal is to minimize the active power curtailment of renewable wind generation and losses while guaranteeing grid constraints at all times.

Providing Auxiliary Services: In addition to the goals of task 1, the wind farms must provide voltage support as an ancillary service. More precisely, the goal is to keep the voltage level at the 225 kV buses below 1.05 p.u.

The benchmark is available online [26], and we invite other researchers to evaluate their control methods on it.

III. ONLINE FEEDBACK OPTIMIZATION WITH INTEGER CONSTRAINTS

In this section, we define the control and optimization setup we choose for the benchmark. Then we present our new OFO controller, and comment on the necessary model information and its tuning before we compare it with Offline Optimization.

A. Input, Output, and Optimization Problem

The input $u = [q^T, p^T, tap^T]^T$ consists of the reactive power setpoints $q \in \mathbb{R}^{42}$ and active power setpoints $p \in \mathbb{R}^{42}$ for the 42 wind parks, and the tap positions $tap \in \mathbb{Z}^{10}$ for the 10 tap changers within the Blocaux area, for a total of 94 signals. The output $y = [v^T, \ell^T]^T$ consists of the voltage magnitudes $v \in \mathbb{R}^{31}$ at the 31 buses and the magnitudes of the complex power flows $\ell \in \mathbb{R}^{58}$, for a total of 89 signals. Let d be the disturbance vector which contains active and reactive power consumptions and the generation that we do not control. The steady-state relation between u , d , and y is determined by the power flow equations. An explicit mapping $y = h(u, d)$ locally exists but its functional form is usually

unknown [27]. The actuators that will implement our control input u are limited in their capabilities and the bus voltages and line flows have lower and upper limits due to safety constraints. Therefore, we introduce a constraint set \mathcal{U} for the input and \mathcal{Y} for the output. The tap changer positions need to be an element of \mathbb{Z} , which is the set of integers. We now formulate an optimization problem, in which the goal is to minimize the losses in the grid and the curtailment that is necessary to satisfy line limits

$$\begin{aligned} \min_{u, y} \quad & f(u, y) := \text{losses}(u, y) + \text{curtailment}(u) \\ \text{s.t.} \quad & y = h(u, d) \\ & u \in \mathcal{U}, \quad y \in \mathcal{Y} \\ & u_i \in \mathbb{Z} \quad \forall \text{ discrete inputs } i \end{aligned} \quad (1)$$

At a local optimum (u^*, y^*) the system satisfies the constraints on u and y , which means that we have a feasible operating point. Furthermore, the cost function is locally minimized. We do not perform frequency control because we consider this to be done at the transmission grid level. For a paper analyzing the interaction of frequency control with OFO, see [18].

B. The Proposed Controller

All proposed OFO controllers cannot handle integer constraints. To solve this issue we build up on work from [28] which we extend with the capabilities to handle discrete inputs and rate limits. The resulting OFO controller is

$$u(k+1) = u(k) + \sigma(u(k), d(k), y_m(k)) \quad (2)$$

$$\begin{aligned} \sigma(u, d, y_m) = \arg \min_{w \in \mathbb{R}^p} \quad & \|w + G^{-1}H(u, d)^T \nabla f(u, y_m)^T\|_G^2 \\ \text{subject to} \quad & A(u + w) \leq b \\ & C(y_m + \nabla_u h(u, d)w) \leq c \\ & w \in \mathcal{W} \\ & w_i \in \mathbb{Z} \quad \forall \text{ discrete inputs } i, \end{aligned} \quad (3)$$

with $H(u, d)^T := [I \quad \nabla_u h(u, d)^T]$ where $\nabla_u h(u, d)$ is the sensitivity of the output with respect to the input and I is the identity matrix. The gradient of the cost function

from (1) is $\nabla f(u, y)$. The set \mathcal{W} can be used to enforce rate constraints on the input u by constraining the change of the input w and G is the tuning matrix. The matrices A and C and vectors b and c are the linearization of \mathcal{U} and \mathcal{Y} from (1) at the current operating point, respectively. Problem (3) is a mixed integer quadratic optimization problem (MIQP) that needs to be solved at every time step. The main difference that makes (3) easier to solve compared to (1) is the lack of the nonlinear equality constraint that describes the power flow equations. The heart of the controller is repeatedly solving this optimization problem. This is similar to sequential quadratic programming (SQP). Essentially, OFO is the real-time feedback version of SQP.

C. Controller Tuning

The tuning of an OFO controller consists of two parts. First, the control objective is encoded in the cost function $f(u, y)$ and constraint sets \mathcal{U} and \mathcal{Y} of the overarching optimization problem (1). Those determine the local optimum that the OFO controller is tracking. Second, the tuning matrix G is used to adjust the transient behavior of how the system is driven to the local optimum. This is explained in more detail in the following two paragraphs.

1) *Tuning the rate of change of different inputs:* The tuning matrix G can be used to tune how the grid is converging to the local optima. The bigger an entry g_i of G is, the less aggressively the corresponding input u_i will be used during the transient. Changing an entry g_i to $g_i + \lambda$ is ultimately equivalent to adding the term λw_i^2 to the cost function in (3) which adds a weight on the change of input i . Without discrete actuators, this only affects how the system converges to the local optimum and not the local optimum itself.

2) *Tuning the tap changer usage:* Tap changer usage comes at a cost because they slowly deteriorate with every tap change. This deterioration is irrelevant when tap changes are needed to enforce constraints. However, one might want to limit the number of tap changes used to minimize the cost function. The proposed OFO controller conveniently provides a tuning option for this which is the matrix G . While G does not affect the constraint enforcement it does affect how often discrete inputs are used. The higher the values in G corresponding to a discrete actuator like tap changers, the less they are used. Numerical results will be shown in Section V.

D. Necessary Model Information

OFO is a mostly model-free approach aside from one key piece of model information: the sensitivity $\nabla_u h(u, d)$ that describes the effect of a change in the input u on the output y . Note, that for example, the sensitivity of power flows (outputs) with respect to active power injections (inputs) are the well-known power-transfer-distribution-factors (PTDFs). Power system sensitivities can be computed with the implicit function theorem using the admittance matrix of the grid, the grid state, and the power flow equations [27]. The sensitivity $\nabla_u h(u, d)$ depends on both u and d and the system parameters, e.g. topology and line impedances. Fortunately, for many applications it can be approximated with a constant

matrix [11]: due to the feedback nature of OFO, the controllers are robust against such approximations and drive the system to an operating point (u, y) that satisfies the constraints and enables the safe operation of the power grid. The suboptimality of this operating point can be bounded [29]. Additionally, there exist methods to learn the sensitivity online from measurements [19]–[21] and there also exist OFO controllers that do not use any sensitivity but instead rely on zeroth order evaluation of the cost [30].

E. Comparison of Offline Optimization and OFO

The key difference between Offline Optimization and OFO is that the former makes decisions based on a model, whereas the latter makes decisions based on a measurement, see Figure 1. With perfect model information, both approaches converge to a locally optimal operation point (u^*, y^*) . For that, Offline Optimization needs to know the sensitivity $\nabla_u h(u, d)$, the model $h(u, d)$, and disturbance d . OFO, instead, only requires the sensitivity $\nabla_u h(u, d)$ because it substitutes the model with a measurement. In the presence of model mismatch, both Offline Optimization and OFO necessarily converge to suboptimal points. When using Offline Optimization this suboptimally can result in constraint violation and potential damage to equipment. OFO controllers instead guarantee constraint satisfaction at steady-state thanks to including repeated measurements as feedback from the system. For a more in-depth comparison between OPF and OFO see Table I. For a comparison with extremum seeking, model predictive control, and modifier adaptation, see [5].

IV. CONTROLLER DESIGN FOR THE BLOCAUX AREA

In this section, we present how the newly proposed algorithm is tailored to the Blocaux area.

A. Constraint Sets and Integer Constraints

The constraint set of the input is $\mathcal{U} = \{u \in \mathbb{R}^{94} \mid u_{min} \leq u \leq u_{max}\}$, where $u_{min} = [q_{min}^T, p_{min}^T, tap_{min}^T]^T$ and $u_{max} = [q_{max}^T, p_{max}^T, tap_{max}^T]^T$. The limits on q and tap are the real grid limits and can be found in the MATPOWER case file of the benchmark [26]. The lower limit for p is $p_{min} = 0$ because the wind farms cannot consume power. The upper limit p_{max} depends on the wind, and we assume that the wind farms provide this information to the controller, see the block diagram in Figure 3. Therefore, the constraints on the active power are different at every time step. An equivalent definition of the constraint set \mathcal{U} is $\mathcal{U} = \{u \in \mathbb{R}^{94} \mid Au \leq b\}$ with $A = [I_{94}, -I_{94}]^T \in \mathbb{R}^{188 \times 94}$, where I_{94} is the identity matrix of size 94, and $b = [u_{max}^T, u_{min}^T]^T \in \mathbb{R}^{128}$. This matrix A and vector b are used in the controller in (3). Note, that we do not include rate limits on the input though this is possible.

The constraint set of the output is $\mathcal{Y} = \{y \in \mathbb{R}^{89} \mid y_{min} \leq y \leq y_{max}\}$, where $y_{min} = [v_{min}^T, \ell_{min}^T]^T$ and $y_{max} = [v_{max}^T, \ell_{max}^T]^T$. The limits on v and ℓ are the real French grid limits for these buses and lines and can be found in the MATPOWER case file of the benchmark [26]. An equal definition of the constraint set \mathcal{Y} is $\mathcal{Y} = \{y \in \mathbb{R}^{89} \mid Cy \leq c\}$

	Offline Optimization	Online Feedback Optimization
Without model mismatch	Locally optimal solution	Same locally optimal solution
With model mismatch	Constraint violations or suboptimal	Constraints are satisfied, converges to the best achievable solution given the model mismatch
Computation	Solving a computationally intense non-convex problem	Calculating an easier update step that is computationally lighter
Tracking behavior	No tracking (only adjusts the inputs when a new estimate of d becomes available)	Tracks the time-varying optimal solution using measurements
Communication infrastructure	Sending setpoints	Sending setpoints & receiving measurements
Control strategy	Feedforward	Feedback
Decision basis	Model-based	Measurement-based
Necessary information	Model $h(u, d)$, disturbance d , and sensitivity $\nabla_u h(u, d)$	Only sensitivity $\nabla_u h(u, d)$

TABLE I: Comparison of Offline Optimization like OPF solvers and Online Feedback Optimization

with $C = [I_{89}, -I_{89}]^T \in \mathbb{R}^{178 \times 89}$, where I_{89} is the identity matrix of size 89, and $c = [y_{max}^T, y_{min}^T]^T \in \mathbb{R}^{178}$. This matrix C and vector c are used in the controller in (3). The tap changers can take 33 discrete positions, and the change of a tap position has to be an integer. When calculating (3) the solver must be informed about these integer constraints on a subset of w . How this is done is solver specific.

B. Sensitivities

The OFO controller needs the sensitivity $\nabla_u h(u, d)$ to drive the system to the optimum. Namely, these are the sensitivities of the outputs v and ℓ with respect to the inputs q , p , and tap . We calculate the sensitivity once initially for a grid state with high power generation and approximate the true time-varying sensitivity with this fixed sensitivity. Note, that the constraints will still be satisfied even with an approximate sensitivity.

C. Cost Function

The cost function encodes our control goal, which is to minimize the losses and the curtailment. This corresponds to the cost function $f(u, y) = losses(u, y) + curtailment(u)$. Furthermore, the regularization of tap changers or other inputs could be added to the cost function. Generally, the cost function specifies how the system is controlled, and it should be chosen judiciously. Note, that for the implementation of the controller only the gradient of the cost function $\nabla f(u, y)$ will be needed, see (3). Note that, Offline Optimization would need this gradient as well. To calculate this gradient an exact model and all active and reactive consumption and generation need to be known. We, therefore, work with an approximate cost function containing only values the controller measures: $f(u, y) = w_q q^2 - sum(p) + \mathbf{w}_{tap} tap$. The term $w_q q^2$ with the scalar weight $w_q = 0.0026$ approximates the losses due to a reactive power flow on a medium voltage line connecting a wind farm to the high voltage grid. The term \mathbf{w}_{tap} is a vector of size 10 and incorporates that higher tap positions lower the losses. It is the derivative of the losses with respect to the tap changer positions. It is calculated once numerically for a grid state with high power generation and kept constant for the whole simulation. The gradient of our approximate cost function is

$$\nabla f(u, y) = \begin{bmatrix} \nabla_u f(u, y) \\ \nabla_y f(u, y) \end{bmatrix} \approx \begin{bmatrix} 2w_q q \\ -I_{42} \\ \mathbf{w}_{tap} \\ 0_{89} \end{bmatrix}.$$

D. Tuning Parameters and Sampling Time

The sampling time of the controller is 1 second. To solve the MIQP in (3) we use the Yalmip toolbox [31] with the solver Gurobi. Solving the MIQP takes less than 40 milliseconds on a standard notebook. As the tuning parameter we choose a diagonal matrix $G = diag(0.1 \cdot I_{42}, 0.2 \cdot I_{42}, 2500 \cdot I_{10})$. The high value of 2500 for the tap changers ensures that they are not overused. The small values for p and q ensure fast convergence of the algorithm.

V. RESULTS

In this section, we use the Unicorn 7019 benchmark to validate our OFO controller and showcase its performance. We show simulations for both tasks (*Optimal and Safe Curtailment* and *Providing Auxiliary Services*). Furthermore, as a benchmark, we simulate our controller with perfect model knowledge to show the effect of the approximations we made. Also, we show the tracking performance of the OFO controller, i.e., how closely it tracks the grand-truth time-varying optimum, and compare it to the state-of-the-art which is curtailing injection at a fixed level. Finally, we present the influence of the tuning matrix G on the tap changer behavior.

A. Results for Optimal and Safe Curtailment

For the task of *Optimal and Safe Curtailment*, we deploy the controller as described in Section IV. The results can be seen in Figure 4, and the behavior can be separated into two phases. In the beginning, the wind power is low and no curtailment is necessary. Therefore, the controller aims to minimize the losses. This is done by increasing the voltage with high tap ratios. To satisfy the voltage constraints not all tap changers increase their tap positions and some reactive power is used. Note that the sharp steps in the reactive power injections (lower left panel) can arise when a tap is changed. These steps in the reactive power are sometimes needed to enforce the voltage constraints when a tap change occurs. Around minute 15 the wind power sharply increases and passes the grid capacity. Curtailment becomes necessary to satisfy the current limits on some of the lines. Even though the tap changers have a small influence on the power flows, this influence is used to redirect flow to non-congested lines. This helps to minimize the necessary curtailment. The tap changes lead to voltages well within the constraints and no reactive power is needed anymore. These are highly non-trivial control actions that no human operator would have been able to derive in real-time. While the wind power increases

the controller curtails more active power to keep the flows within the constraints. It can be seen in Figure 4 that line constraints violations are minimal and most importantly they are temporary. Therefore, the grid is safely operated at its limit allowing a maximum of renewable wind power to be injected. At the end of the simulation 90.2% of the wind power is injected into the grid.

As explained before, the OFO controller is tracking the locally optimal solution of the optimization problem defined in Section IV. We have a high cost on active power curtailment and therefore this control action is only used if it is necessary to satisfy line constraints or in the unlikely case that such a high amount of reactive power would need to be used to satisfy voltage limits that a lower value of the cost function could be achieved by curtailing active power. If another behavior is wanted this can be encoded in the cost function.

B. Results for Providing Auxiliary Services

In this task the subtransmission grid has to provide voltage support to the transmission grid as an ancillary service. The goal is to keep the voltages at the 225 kV buses below 1.05 p.u. This can easily be incorporated into our controller by changing the upper voltage constraint of these buses to 1.05. This example shows the versatility of our framework, i.e., defining the control goals through an optimization problem. The results of the simulation can be seen in Figure 5. Similar to the previous task the behavior is split into two phases. In the beginning, the losses are minimized and after minute 15 the focus lies on optimizing curtailment as it becomes the predominant part of the cost. The main difference to the previous task is in the usage of the tap changers and reactive power to satisfy the tighter voltage constraints on the 225 kV buses. For that, more reactive power is used and the tap changers are actuated more. After minute 15 the tap changers behave differently than in the previous task because of the tighter voltage constraints. This leads to a slightly higher curtailment and reactive power is still needed to enforce the voltage constraints. At the end of the simulation 89.9% of the wind power can be injected into the grid.

C. The Effect of the Approximations

When designing the controller in Section IV we assumed that the sensitivity $\nabla_u h(u, d)$ and the derivative of the cost function $\nabla f(u, y)$ are not perfectly known, which is always the case in a practical application. This imperfection affects the optimality of the time-varying state the controller is tracking. To analyze the sub-optimality we run our OFO controller for *Optimal and Safe Curtailment* again but with perfect information about the sensitivity and derivative of the cost function at every time step. The main difference is in the usage of reactive power and the tap changers, see Figure 6. The active power curtailment however is very similar. This is because the approximation of the derivative of the cost function with respect to curtailment is highly accurate as well as the sensitivity of the line flows with respect to the curtailment (those are PTDFs). Overall, 91.14% of the available wind power can be used. This is mostly due to

using the reactive power capabilities to reduce reactive power flows on the saturated lines and therefore freeing up capacity for active power flows. Also, the reactive power capabilities are used to reduce reactive power flows in general to lower the losses in the grid. Again, we want to highlight that the suboptimality under model mismatch does not arise from the method but is fundamental to the problem of making decisions based on inaccurate information. Nevertheless, OFO guarantees constraint satisfaction in steady-state while other methods do not.

D. Tracking Performance & Comparison to Ground Truth

Changes in the consumption or the production affect the optimal solution of the optimization problem and an OFO controller is constantly trying to track this time-varying local optimum. To analyze the tracking performance we calculate the time-varying optimal solution with an OPF solver that has perfect model knowledge. For a fair comparison, we also provide the OFO controller with perfect model knowledge. We solve the task *Optimal and Safe Curtailment* with both approaches and plot the wind power that they can use. To be able to run the MATPOWER OPF solver we block the tap changers in the Blocaux area at 1. To have a fair comparison we also block the tap changers at 1 for the OFO controller. The result can be seen in Figure 7, and show that the optimality of the OFO controller is practically identical to the theoretical optimum that we compute with an omniscient and instantaneous OPF solver. The figure also shows a comparison with the state-of-the-art which is curtailing the wind farms at a fixed level. Here we chose 60% which already leads to one line being loaded at close to 90% meaning that the remaining headroom, for potential lower consumption in the Blocaux and therefore higher line loads, is small. From the figure it becomes apparent that at full wind output, the OFO controller allows the wind farms to inject 50 % more power than the state-of-the-art. The reason behind this large number is that not all lines become saturated and therefore only a few wind parks need to be curtailed. Due to the feedback from the grid, the OFO controller can optimally solve this non-trivial task of deciding which wind park has to be curtailed by which value at what time while making sure all voltages and lines are within their limits.

E. Tap changer behavior

The tuning matrix G influences the tap changer behavior. To illustrate this behavior, we simulate the benchmark for different G . More precisely, we use the controller for *Optimal and Safe Curtailment* and change the entries of G corresponding to tap changers. The results for different values can be seen in Figure 8. With a value of 500, the tap changers are heavily used and might deteriorate quickly. For larger values, their usage decreases and with the value 5000 they are only used once the grid reaches its capacity limit. With a much larger value than 5000, the tap changers would not be used at all unless needed to enforce operational constraints, e.g. voltage limits.

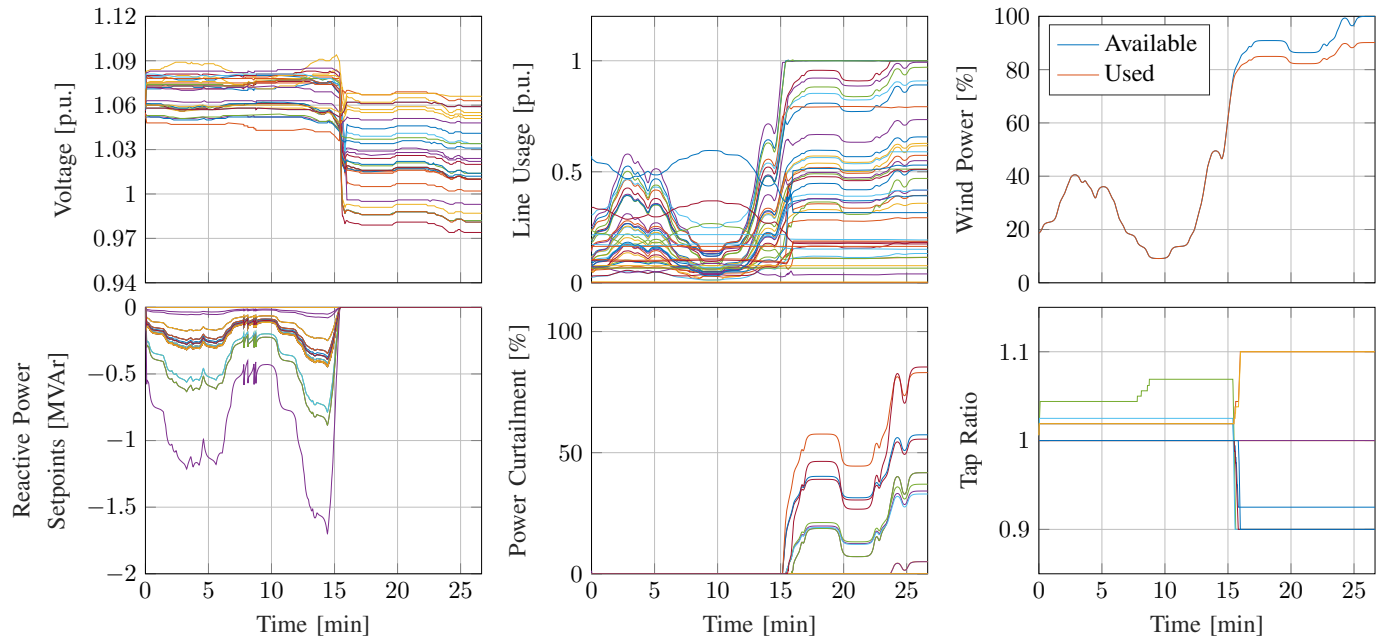


Fig. 4: Simulation of the Unicorn benchmark under time-varying wind power (blue line in top right plot). The lower three plots show the control inputs and the upper plots show the resulting voltages, line usage, and used wind power. The voltage constraints that the controller has to enforce are the real French grid limits.

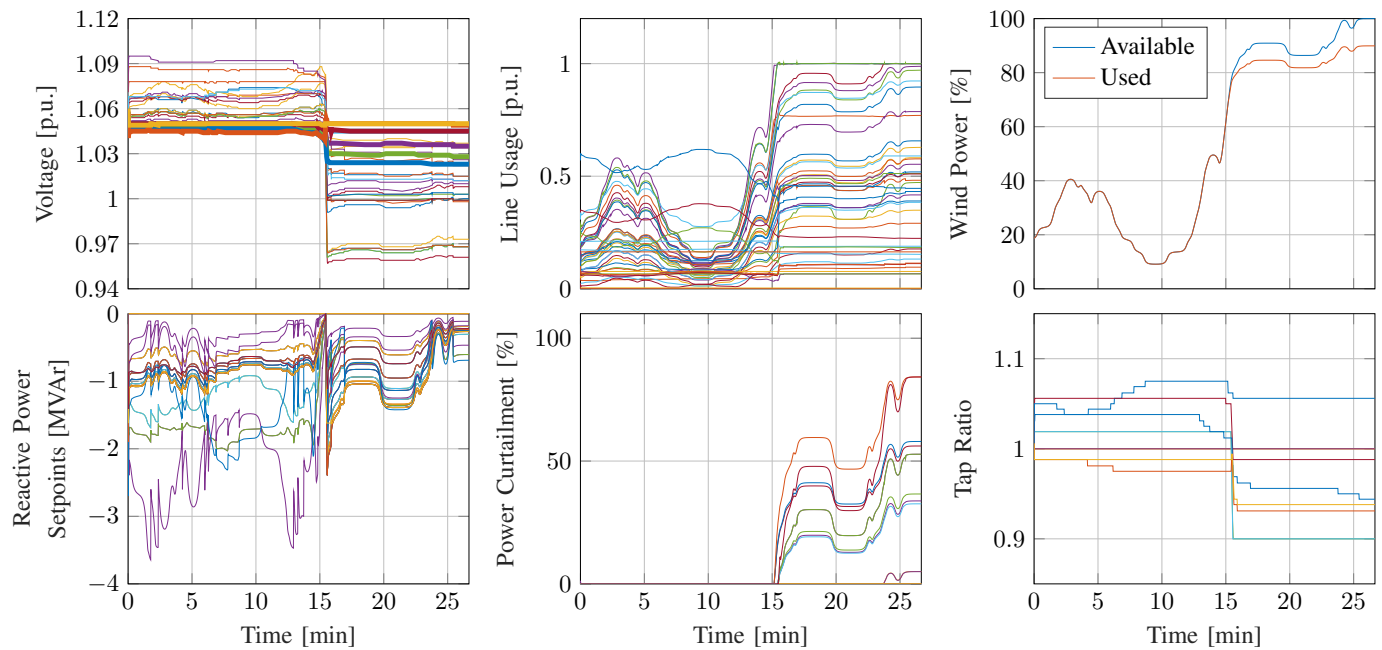


Fig. 5: Simulation of the Unicorn benchmark under time-varying wind power (blue line in top right plot). The lower three plots show the control inputs and the upper plots show the resulting voltages, line usage, and used wind power. The voltage constraints of the 225 kV buses were set to 1.05 p.u. Those buses are indicated with a thicker line. The controller is enforcing these limits.

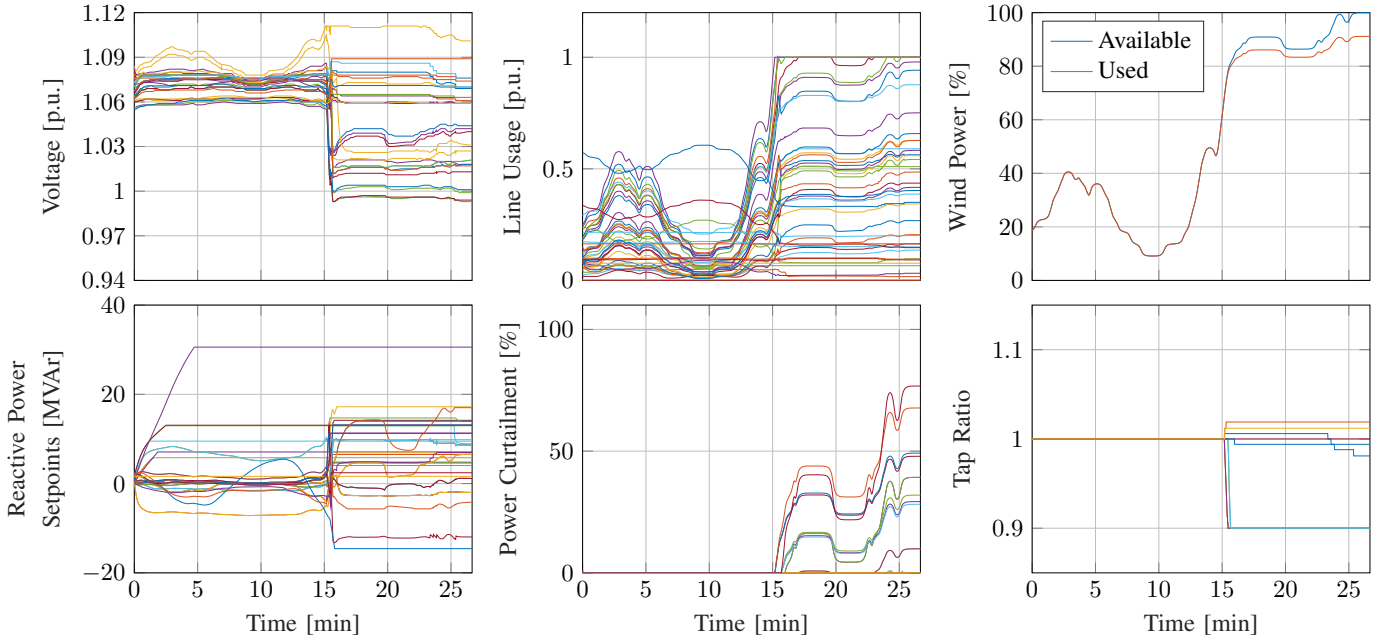


Fig. 6: Simulation of the Unicorn benchmark under time-varying wind power (blue line in top right plot). The lower three plots show the control inputs and the upper plots show the resulting voltages, line usage, and used wind power. In this simulation, the controller has perfect knowledge of the sensitivity $\nabla_u h(u, d)$ and the derivative $\nabla f(u, y)$.

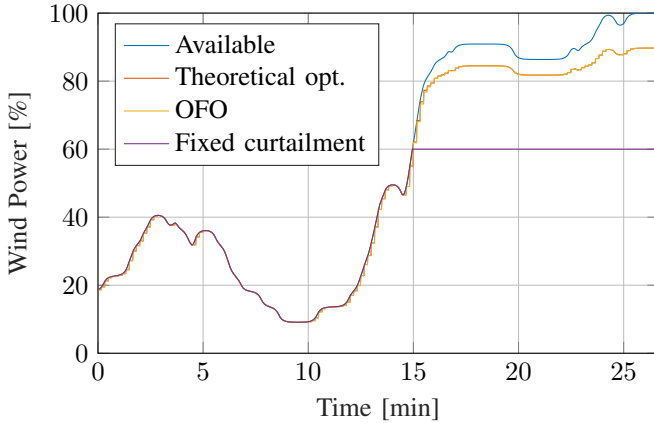


Fig. 7: Comparison of the available wind power, the wind power that can be theoretically used, fixed curtailment at 60%, and the wind power that the OFO controller can use.

VI. CONCLUSION

By extending OFO controllers with the capability to handle discrete actuators, we are able to design a real-time controller for a real subtransmission grid benchmark that uses a diverse range of actuators, i.e., active and reactive power capabilities and on-load tap changers. Moreover, this controller operates the grid safely at the locally optimal operation point and tracks the local optimum when it changes over time. We were able to show that this tracking is highly precise and not sensitive to model mismatch. This leads to the OFO controller being able to extract 50% more wind power in the benchmark than the state-of-the-art. Furthermore, we showed that specifying control objectives in an optimization problem is versatile and

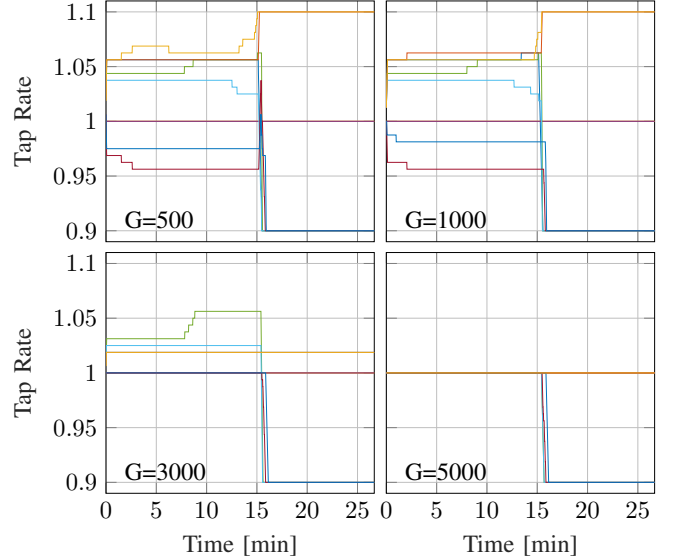


Fig. 8: Behavior of the tap changers for different values of the entries of G corresponding to the tap changers.

allows us to easily include ancillary services like voltage control. Most importantly, however, the simulations on the real benchmark show that OFO can be a powerful tool to safely operate the subtransmission grid in real-time, under model mismatch, and with limited model information. A remaining open question is how several independently controlled subtransmission grids would interact with each other.

REFERENCES

- [1] “World energy outlook 2021,” IEA, Tech. Rep., 2021. [Online]. Available: <https://www.iea.org/reports/world-energy-outlook-2021>
- [2] “Renewable energy statistics 2022,” The International Renewable Energy Agency, Tech. Rep., 2022.
- [3] “Schéma décennal de développement du réseau (sddr) 2019 - rapport complet,” RTE Réseau de transport d’électricité, Tech. Rep., 2019. [Online]. Available: <https://www.rte-france.com/analyses-tendances-et-prospectives/le-schema-decennal-de-developpement-du-reseau#Documents>
- [4] D. K. Molzahn, F. Dörfler, H. Sandberg, S. H. Low, S. Chakrabarti, R. Baldick, and J. Lavaei, “A survey of distributed optimization and control algorithms for electric power systems,” *IEEE Transactions on Smart Grid*, vol. 8, no. 6, pp. 2941–2962, 2017.
- [5] A. Hauswirth, S. Bolognani, G. Hug, and F. Dörfler, “Optimization algorithms as robust feedback controllers,” *arXiv:2103.11329*, 2021.
- [6] A. Bernstein, E. Dall’Anese, and A. Simonetto, “Online primal-dual methods with measurement feedback for time-varying convex optimization,” *IEEE Trans. Signal Process.*, vol. 67, no. 8, pp. 1978–1991, 2019.
- [7] L. S. Lawrence, J. W. Simpson-Porco, and E. Mallada, “Linear-convex optimal steady-state control,” *IEEE Transactions on Automatic Control*, vol. 66, no. 11, pp. 5377–5384, 2020.
- [8] M. Colombino, E. Dall’Anese, and A. Bernstein, “Online optimization as a feedback controller: Stability and tracking,” *IEEE Transactions on Control of Network Systems*, vol. 7, no. 1, pp. 422–432, 2019.
- [9] G. Bianchin, J. Cortes, J. I. Poveda, and E. Dall’Anese, “Time-varying optimization of lti systems via projected primal-dual gradient flows,” *IEEE Transactions on Control of Network Systems*, 2021.
- [10] A. Simonetto, E. Dall’Anese, S. Paternain, G. Leus, and G. B. Giannakis, “Time-varying convex optimization: Time-structured algorithms and applications,” *Proceedings of the IEEE*, vol. 108, no. 11, pp. 2032–2048, 2020.
- [11] L. Ortmann, A. Hauswirth, I. Caduff, F. Dörfler, and S. Bolognani, “Experimental validation of feedback optimization in power distribution grids,” *Electric Power Systems Research*, vol. 189, p. 106782, 2020.
- [12] L. Ortmann, A. Prostejovsky, K. Heussen, and S. Bolognani, “Fully distributed peer-to-peer optimal voltage control with minimal model requirements,” *Electric Power Systems Research*, vol. 189, p. 106717, 2020.
- [13] B. Kroposki, A. Bernstein, J. King, and F. Ding, “Good grids make good neighbors,” *IEEE Spectrum*, vol. 57, no. NREL/JA-5D00-78521, 2020.
- [14] S. Li, W. Wu, and Y. Lin, “Robust data-driven and fully distributed volt/var control for active distribution networks with multiple virtual power plants,” *IEEE Transactions on Smart Grid*, vol. 13, no. 4, pp. 2627–2638, 2022.
- [15] G. Qu and N. Li, “Optimal distributed feedback voltage control under limited reactive power,” *IEEE Transactions on Power Systems*, vol. 35, no. 1, pp. 315–331, 2019.
- [16] H. J. Liu, W. Shi, and H. Zhu, “Distributed voltage control in distribution networks: Online and robust implementations,” *IEEE Transactions on Smart Grid*, vol. 9, no. 6, pp. 6106–6117, 2017.
- [17] Y. Guo, X. Zhou, C. Zhao, L. Chen, G. Hug, and T. H. Summers, “An online joint optimization–estimation architecture for distribution networks,” *IEEE Transactions on Control Systems Technology*, 2023.
- [18] J. C. Olives-Camps, Á. R. del Nozal, J. M. Mauricio, and J. M. Maza-Ortega, “A holistic model-less approach for the optimal real-time control of power electronics-dominated ac microgrids,” *Applied Energy*, vol. 335, p. 120761, 2023.
- [19] A. D. Dominguez-Garcia, M. Zholbaryssov, T. Amuda, and O. Ajala, “An online feedback optimization approach to voltage regulation in inverter-based power distribution networks,” *arXiv preprint arXiv:2303.08164*, 2023.
- [20] S. Nowak, Y. C. Chen, and L. Wang, “Measurement-based optimal der dispatch with a recursively estimated sensitivity model,” *IEEE Transactions on Power Systems*, vol. 35, no. 6, pp. 4792–4802, 2020.
- [21] M. Picallo, L. Ortmann, S. Bolognani, and F. Dörfler, “Adaptive real-time grid operation via online feedback optimization with sensitivity estimation,” *Electric Power Systems Research*, vol. 212, p. 108405, 2022.
- [22] Z. Tang, E. Ekomwenrenren, J. W. Simpson-Porco, E. Farantatos, M. Patel, and H. Hooshyar, “Measurement-based fast coordinated voltage control for transmission grids,” *IEEE Transactions on Power Systems*, vol. 36, no. 4, pp. 3416–3429, 2020.
- [23] Z. Tang, D. J. Hill, and T. Liu, “Distributed coordinated reactive power control for voltage regulation in distribution networks,” *IEEE Transactions on Smart Grid*, vol. 12, no. 1, pp. 312–323, 2020.
- [24] R. D. Zimmerman, C. E. Murillo-Sánchez, and R. J. Thomas, “Matpower: Steady-state operations, planning, and analysis tools for power systems research and education,” *IEEE Transactions on power systems*, vol. 26, no. 1, pp. 12–19, 2010.
- [25] L. Ortmann, “Github repository,” <https://github.com/Lukas738/SimulinkMATPOWER>, 2023.
- [26] —, “Gitlab repository,” <https://gitlab.ethz.ch/ortmann/online-feedback-optimization-for-transmission-grid-operation>, 2022.
- [27] S. Bolognani and F. Dörfler, “Fast power system analysis via implicit linearization of the power flow manifold,” in *53rd Annual Allerton Conference on Communication, Control, and Computing (Allerton)*, 2015, pp. 402–409.
- [28] V. Häberle, A. Hauswirth, L. Ortmann, S. Bolognani, and F. Dörfler, “Non-convex feedback optimization with input and output constraints,” *IEEE Control Systems Letters*, vol. 5, no. 1, pp. 343–348, 2020.
- [29] M. Colombino, J. W. Simpson-Porco, and A. Bernstein, “Towards robustness guarantees for feedback-based optimization,” in *58th Conference on Decision and Control (CDC)*, 2019, pp. 6207–6214.
- [30] Z. He, S. Bolognani, J. He, F. Dörfler, and X. Guan, “Model-free nonlinear feedback optimization,” *arXiv:2201.02395*, 2022.
- [31] J. Lofberg, “Yalmip: A toolbox for modeling and optimization in matlab,” in *IEEE International Conference on Robotics and Automation*, 2004, pp. 284–289.